Langmuir

Article

pubs.acs.org/Langmuir

Colloid Interaction Energies for Physically and Chemically Heterogeneous Porous Media

Scott A. Bradford*[,†] and Saeed Torkzaban[‡]

[†]US Salinity Laboratory, USDA, ARS, Riverside, California 92507, United States

[‡]CSIRO Land and Water, Glen Osmond, SA 5064, Australia

ABSTRACT: The mean and variance of the colloid interaction energy (Φ^*) as a function of separation distance (h) were calculated on physically and/or chemically heterogeneous solid surfaces at the representative elementary area (REA) scale. Nanoscale roughness was demonstrated to have a significant influence on the colloid interaction energy for different ionic strengths. Increasing the roughness height reduced the magnitude of the energy barrier (Φ_{max}^*) and the secondary minimum (Φ_{2min}^*). Conversely, increasing the fraction of the solid surface with roughness increased the magnitude of Φ_{max}^* and Φ_{2min}^*. Our results suggest that primary minimum interactions tend to occur in cases where only a portion of the solid surface was covered with roughness (i.e., isolated roughness pillars), but their depths were shallow as a result of Born repulsion. The secondary minimum was strongest on smooth surfaces. The variance in the interaction energy was also a strong function of roughness parameters and h. In particular, the variance tended to increase with the colloid size, the magnitude of Φ^*, the height of the roughness, and especially the size (cross-sectional area) of the heterogeneity. Nonzero values of the variance for Φ_{2min}^* implied the presence of a tangential component of the adhesive force and a resisting torque that controls immobilization and release for colloids at this location. Heterogeneity reduced the magnitude of Φ^* in comparison to the corresponding homogeneous situation. Physical heterogeneity had a greater influence on mean properties of Φ^* than similar amounts of chemical heterogeneity, but the largest reduction occurred on surfaces with both physical and chemical heterogeneity. The variance in Φ^* tended to be higher for a chemically heterogeneous solid.

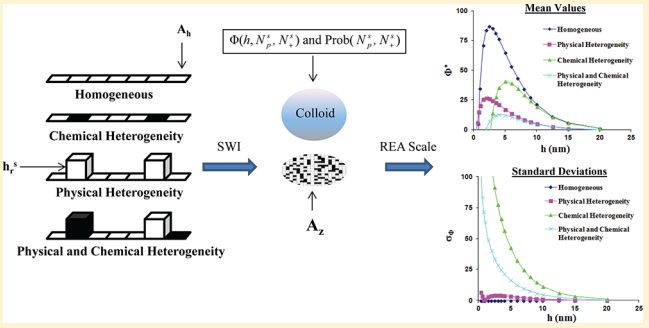

INTRODUCTION

Colloid interactions with surfaces play a critical role in many industrial and environmental applications. Derjaguin−Landau−Verwey−Overbeek (DLVO) theory[1,2] has been extensively employed to determine colloid interaction energies as the sum of van der Waals and electrostatic interactions. However, numerous deviations from standard DLVO predictions have been reported, especially in the presence of net repulsive electrostatic interactions.[3−23] These deviations have been attributed to intrinsic assumptions in DLVO theory regarding the controlling interactions and geometrically smooth and chemically homogeneous surfaces.[4−8,10,14,16,23] For example, DLVO theory sometimes needs to be extended to account for Born repulsion, steric interactions, hydrophobic interactions, and/or hydration effects.[24] Other researchers have employed surface integration approaches in conjunction with DLVO theory to account for the influence of microscopic physical and/or chemical heterogeneity on interaction energies.[4−8,10,14,16,23]

Natural solid surfaces and colloids exhibit some degree of roughness at small scales.[3] Surface integration calculations have demonstrated that microscopic surface roughness can reduce or eliminate the DLVO interaction energy barrier under unfavorable attachment conditions.[3,5−7] Primary minima interactions have been reported to sometimes occur on top of surface roughness protrusions, especially at higher ionic strength (IS).[7,19,20,23] Conversely, pits and sides of surface roughness have been reported to increase the depth of the secondary minima.[7,19,23] Indeed, colloid deposition has been found to increase on rough surfaces in atomic force microscopy studies,[25,26] in parallel flow chamber experiments,[27,28] and in column-scale transport investigations.[29,30] Reversible secondary and/or primary minimum interactions may occur on rough surfaces with a reduction in solution IS depending the colloid size.[19−23,31,32]

The above information indicates that colloid interactions with surfaces will be strongly dependent on surface roughness properties (e.g., height, size, and numbers) and that these effects will depend on the colloid size and solution IS. However, surface integration studies have typically been limited to very small spatial scales because they are very computationally intensive. Our understanding and ability to quantify the influence of surface roughness on colloid interactions is still incomplete, especially at larger spatial scales. Upscaled

Received: January 17, 2013
Revised: February 22, 2013
Published: February 25, 2013

   dx.doi.org/10.1021/la400229f | Langmuir 2013, 29, 3668−3676

information on colloid interactions is needed at the representative elementary volume (REV) and/or area (REA) scales for continuum transport models which are used for numerous real-world applications.[32−36] Furthermore, colloid interactions will exhibit a distribution on physically heterogeneous (rough) surfaces at the REV scale. Consequently, spatial variations in colloid adhesive properties are expected, and only a fraction of the solid surface area may contribute to colloid immobilization.[16,37]

In addition to physical heterogeneity (roughness), microscopic chemical heterogeneities have been reported to contribute to colloid retention under unfavorable attachment conditions.[10−17,37] Microscopic chemical heterogeneity may occur on natural colloid and solid surfaces as a result of mineral defects, isomorphic substitution, protonation/deprotonation of hydroxyl groups, and adsorption of different ions, organics, and clay particles.[38−40] The presence of both microscopic physical (roughness) and chemical heterogeneity is therefore expected to simultaneously contribute to colloid interactions. However, very limited research has addressed the combined influence of physical and chemical heterogeneity on colloid interactions, especially at the REV scale. Bendersky and Davis[16] reported that the influence of surface roughness increased when the tops of pillars (representing roughness) had a different zeta potential than the underlying surface. Duffadar and Davis[12] examined colloid trajectories over a surface with nanoscale chemical heterogeneities and 2 nm surface protrusions. Zhang et al.[41] demonstrated that colloid immobilization in the presence of fluid flow depended on the size and height of nanoscale heterogeneities.

Bradford and Torkzaban[37] presented a method to determine colloid interaction energies on chemically heterogeneous surfaces at the REV scale. We extend this method in this work to consider the influence of physical and/or chemical heterogeneity on colloid interactions at the REV scale and validate our approach through comparison with published grid surface integration calculations. Numerical simulations provide insight into colloid interactions on surfaces with various degrees of roughness (height, number, and size) and chemical heterogeneity under different solution IS conditions.

THEORY

Physical Heterogeneity on the Solid−Water Interface.

Similar to Bendersky and Davis,[16] physical heterogeneity is represented in this work as nanoscale pillars of a given cross-sectional area (A_h, L^2) and height (h_r^s, L) that are randomly distributed on the solid−water interface (SWI). The colloid−SWI interaction energy depends on its spatial location and distance from the SWI and pillars. However, only a portion of the SWI contributes to the colloid−SWI interaction energy, and this area is known as the zone of electrostatic influence (A_z, L^2). The value of A_z is given as[12]

$$A_z \cong \frac{4\pi r_c}{\kappa} \tag{1}$$

where r_c $[L]$ is the colloid radius and κ $[L^{-1}]$ is the Debye−Huckel parameter. The relationship between κ^{-1} and the IS of a 1:1 electrolyte solution is given as $\kappa^{-1} = 0.301(\mathrm{IS})^{-0.5}$, where κ^{-1} is in units of nm and IS has units of M.[12] To account for the heterogeneous distribution of pillars within A_z, this region is discretized into a number of equally sized cells. The cross-sectional area of each cell size is equal to A_h, and the total number of cells (N_t) is equal to the ratio of A_z to A_h. Each cell is associated with a surface roughness height equal to 0 or h_r^s.

Grid surface integration (GSI) calculations (average of 200) indicated that the mean dimensionless (divided by the product of the Boltzmann constant, k_B, and the absolute temperature, T_K) interaction energy (Φ) on a physically heterogeneous surface is given by a linear combination of the dimensionless interaction energies associated with the pillar tops and the underlying SWI.[16] The dimensionless interaction energy on a smooth SWI (Φ_S) can be used to determined similar values for cells with and without pillars. The only difference in Φ_S on cells with and without pillars is in their separation distance from the colloid. Consequently, the mean value of Φ within A_z is determined as[16]

$$\Phi(h) = \left(1 - \frac{N_p^s}{N_t}\right)\Phi_S(h + h_r^s) + \frac{N_p^s}{N_t}\Phi_S(h) \tag{2}$$

where h is the separation distance from the leading face of the colloid center to the pillar top and N_p^s is the number of cells that are associated with pillars. It should be mentioned that eq 2 is consistent with results from other surface integration techniques reported in the literature.[8,19,20] Values of Φ_S were calculated as the sum of interactions arising from electrostatics,[42] retarded London−van der Waals attraction,[43] and Born repulsion.[44] Other non-DLVO interactions (e.g., steric forces, hydrophobic forces, and hydration effects) were not considered in this analysis. A sphere−plate geometry was assumed in eq 2, and zeta potentials (ζ) were used in place of surface potentials. Consequently, values of $\Phi(h)$ through this work are implicit functions of κ, colloid and SWI zeta potentials, the colloid radius, the Hamaker constant, the characteristic wavelength, and the collision diameter.

Mean values of $\Phi(h)$ were calculated for possible realizations of physical heterogeneity (N_p^s = 0, 1, ..., N_t) within A_z using eq 2; h ranged from 0.1 to 20 nm in 0.1 nm increments. Note that the particular location of a pillar within A_z is not needed to determine these statistically mean values.[16] The energy barrier height (Φ_{max}), the depth of the secondary minimum (Φ_{2min}), and the depth of the primary minimum (Φ_{1min}) were determined for each of these physical heterogeneity realizations using Boolean logic statements in conjunction with minimum and/or maximum functions over specified intervals in h.

The above information describes the determination of mean values of $\Phi(h)$, Φ_{2min}, Φ_{1min}, and Φ_{max} for possible physical heterogeneity realizations (N_p^s = 0, 1, ..., N_t) within A_z. Additional information is needed to determine the probability density functions (PDFs) for these interaction energy parameters on a physically heterogeneous porous medium at the REA scale. If the total fraction of cells that is occupied by pillars on the SWI is known at the REA scale of a porous medium (P_p^s) and the pillars are randomly distributed, then the probability for the occurrence of each physical heterogeneity realization (Prob(N_p^s)) within A_z is obtained from the binomial mass distribution as

$$\mathrm{Prob}(N_p^s) = \frac{N_t!}{N_p^s!(N_t - N_p^s)!}(P_p^s)^{N_p^s}(1 - P_p^s)^{N_t - N_p^s} \tag{3}$$

The associated PDFs for $\Phi(N_p^s)$ at selected values of h, $\Phi_{2min}(N_p^s)$, $\Phi_{1min}(N_p^s)$, and $\Phi_{max}(N_p^s)$, at the REA scale of a porous medium are obtained by plotting versus Prob(N_p^s). It

dx.doi.org/10.1021/la400229f | Langmuir 2013, 29, 3668−3676

follows that the mean value of Φ_{2min} on the entire heterogeneous surface at the REA scale is given as

$$\Phi_{2min}{}^{*} = \langle \Phi_{2min} \rangle = \sum_{N_p^s=0}^{N_t} \mathrm{Prob}(N_p^s)\Phi_{2min}(N_p^s) \quad (4)$$

Here the asterisk is used to denote the mean value of a given parameter at the REA scale. The variance of $\Phi_{2min}{}^{*}$ is given as $\langle \Phi_{2min}{}^{2} \rangle - \langle \Phi_{2min} \rangle^2$, and the associated standard deviation is equal to the square root of the variance.[45] Similar expressions were used to determine the mean, variance, and standard deviation of Φ_{max}, Φ_{1min}, and/or $\Phi(h)$ at the REV scale by replacing $\Phi_{2min}{}^{*}$ and Φ_{2min} terms in eq 4.

Physical and Chemical Heterogeneity on the SWI. Similar to GSI simulations, we assume below that A_h is selected to represent the smallest sized physical or chemical heterogeneity of interest in the SWI. The simplest form of chemical and physical heterogeneity is introduced into eq 2 by assigning different ζ values to cells with (ζ_T^s, mV) and without pillars (ζ_B^s, mV). These values of ζ_T^s and ζ_B^s were subsequently used to calculate the dimensionless interaction energy on cells with (Φ_T) and without (Φ_B) pillars, respectively. In this case, eq 2 is rewritten as

$$\Phi(h) = \left(1 - \frac{N_p^s}{N_t}\right)\Phi_B(h + h_r^s) + \frac{N_p^s}{N_t}\Phi_T(h) \quad (5)$$

Equations 1, 3, and 4 are again used to determine interaction energy parameters at the REA scale.

A different approach needs to be taken when the chemical heterogeneity is randomly distributed on the SWI. The mean value of Φ_S within A_z is determined as[16]

$$\Phi_S(h) = \left(1 - \frac{N_+^s}{N_t}\right)\Phi_-(h) + \frac{N_+^s}{N_t}\Phi_+(h) \quad (6)$$

where N_+^s is the number of cells with a positive zeta potential (ζ_+^s) and ($N_t - N_+^s$) is the number of cells with a negative zeta potential (ζ_-^s). Values of ζ_-^s and ζ_+^s were used to determine $\Phi_-(h)$ and $\Phi_+(h)$, respectively. Consequently, the mean value of $\Phi(h)$ within A_z on a physically and chemically heterogeneous SWI is given by eq 2 using eq 6 to determine Φ_S.

The probability for each physical and chemical heterogeneity realization on the SWI at the REA scale is given by the joint binomial mass distribution as

$$\mathrm{Prob}(N_p^s, N_+^s) = \mathrm{Prob}(N_p^s)\,\mathrm{Prob}(N_+^s) \quad (7)$$

Here $\mathrm{Prob}(N_+^s)$ is given analogously to eq 3 but with N_+^s and P_+^s replacing N_p^s and P_p^s, respectively, where P_+^s is the total fraction of cells on the SWI at the REA scale with ζ_+. Equation 7 assumes that physical and chemical heterogeneity on the SWI act independently of each other.

The associated probability density function for $\Phi_{2min}(N_p^s,N_+^s)$ at the REA scale is obtained by plotting versus $\mathrm{Prob}(N_p^s,N_+^s)$ (eqs 3 and 7). In this case, $\Phi_{2min}(N_p^s,N_+^s)$ was derived from $\Phi(h)$ that was determined using eq 5 (different zeta potentials on the tops and bottoms of pillars) or eqs 2 and 6 (random physical and chemical heterogeneity). It follows that the mean value of Φ_{2min} on the entire physically and chemically heterogeneous SWI at the REA scale, $\langle \Phi_{2min} \rangle$, is given as

$$\Phi_{2min}^{*} = \sum_{N_p^s=0}^{N_t}\sum_{N_+^s=0}^{N_t} \mathrm{Prob}(N_p^s, N_+^s)\Phi_{2min}(N_p^s, N_+^s) \quad (8)$$

The variance of $\Phi_{2min}{}^{*}$ is again given as $\langle \Phi_{2min}{}^{2} \rangle - \langle \Phi_{2min} \rangle^2$, and the associated standard deviation is equal to the square root of the variance.[45] Similar expressions were used to determine the mean, variance, and standard deviation of Φ_{max}, Φ_{1min}, and/or $\Phi(h)$ at the REA scale by replacing the Φ_{2min} and $\Phi_{2min}{}^{*}$ terms in eq 8.

RESULTS AND DISCUSSION

Numerical simulations are presented below to investigate the influence of microscopic surface roughness or the combined influence of surface roughness and chemical heterogeneity on $\Phi^*(h)$. The Hamaker constant equaled 5×10^{-21} J, the characteristic wavelength was 100 nm, and the zeta potential of the colloid (ζ^c) was −27 mV in these simulations. The collision diameter that was used to calculate Born repulsion was set equal to 0.5 nm.[24]

Model Validation. Bendersky and Davis[16] conducted multiple GSI simulations (~200) on a randomly generated physically heterogeneous SWI in which the zeta potentials for pillar tops and bottoms were different. Specific parameter values used in these GSI simulations included ζ_T^s = 54 mV and ζ_B^s = −27 mV, IS = 5.8 mM (κ^{-1} = 4 nm), r_c = 500 nm, A_z = 25133 nm^2, A_h = 78.5 nm^2, P_p^s = 0.196, and h_r^s = 1 nm. Figure 1 presents our simulation model output (eqs 1 and 3−5) for Φ^* as a function of h using equivalent properties for the physically and chemically heterogeneous SWI. The error bars in this figure represent ±1.5 standard deviations of Φ^*. The value of $\Phi_{max}{}^{*}$ = 14 and $\Phi_{2min}{}^{*}$ = 0.25 in Figure 1. The mean values and error bars shown in Figure 1 are very similar to that reported by Bendersky and Davis,[16] providing a qualitative validation of our simplified modeling approach on a physically and chemically heterogeneous SWI. It should be mentioned that we have employed a different model for van der Waals interactions than Bendersky and Davis.[16] Consequently, slight differences in the simulation results are to be expected. However, nearly identical simulation results could be achieved by adjusting a single

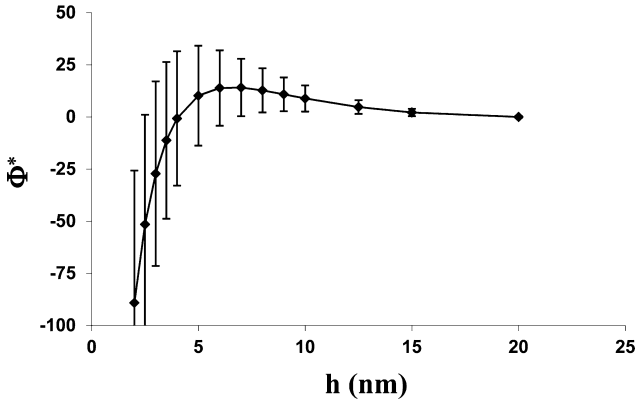

Figure 1. Predicted values of Φ^* as a function of h (eqs 1 and 3−5) for the physically and chemically heterogeneous SWI described by Bendersky and Davis.[16] Model parameters included ζ_T^s = 54 mV and ζ_B^s = −27 mV, IS = 5.8 mM (κ^{-1} = 4 nm), r_c = 500 nm, A_z = 25 133 nm^2, A_h = 78.5 nm^2, P_p^s = 0.196, and h_r^s = 1 nm. The error bars in this figure represent ±1.5 standard deviations of Φ^*.

dx.doi.org/10.1021/la400229f | Langmuir 2013, 29, 3668−3676

parameter (the characteristic wavelength) in our selected model for retarded London−van der Waals interactions.[43]

Physical Heterogeneity on the SWI. Figure 2 presents plots of Φ* as a function of h for various h_r^s (0, 1, 2.5, 5, and 10 nm) and IS (5.8, 50, and 100 mM). Specific parameter values used in these simulations included a zeta potential of the SWI (ζ^s) equal to −11.1 mV, r_c = 500 nm, A_h = 78.5 nm^2, and P_p^s = 0.196. As expected, the magnitudes of Φ_{max}* and Φ_{2min}* decreased and increased, respectively, with increasing IS because of compression of the double-layer thickness. Observe that as h_r^s increased, the magnitudes of Φ_{max}* and Φ_{2min}* decreased. Similar behavior has been reported in the literature.[3,5−7] This decrease in Φ_{max}* and Φ_{2min}* with h_r^s has been attributed to increased van der Waals attraction at smaller separation distances and increased electrostatic repulsion at larger separation distances, respectively.[3] Furthermore, increasing h_r^s sometimes produced nonmonotonic changes in Φ* in the absence of an repulsive interaction energy (Figure 2c). Similar to unfavorable attachment conditions, this implies that colloids may diffuse over an energy barrier under favorable attachment conditions to obtain a stronger interaction in Φ_{1min}*. This observation may help explain increased resistance to detachment with reductions in solution IS with increasing deposition aging time.[46,47]

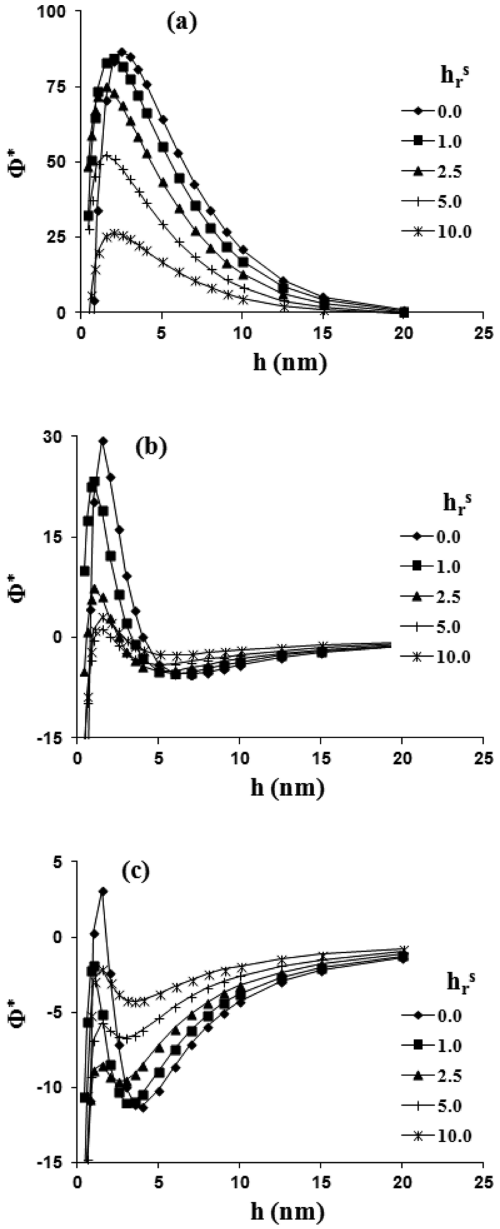

Figure 2. Simulated values of Φ* as a function of h for various h_r^s (0, 1, 2.5, 5, and 10 nm). The IS was 5.8 mM in (a), 50 mM in (b), and 100 mM in (c). Parameter values used in these simulations included r_c = 500 nm, ζ^s = −11.1 mV, A_h = 78.5 nm^2, and P_p^s = 0.196.

Figure 3 presents plots of Φ* as a function of h for various P_p^s (0.05, 0.1, 0.2, 0.4, and 0.6) and IS (5.8, 50, and 100 mM). Specific parameter values used in these simulations included ζ^s = −11.1 mV, r_c = 500 nm, A_h = 78.5 nm^2, and h_r^s = 10 nm. Equation 2 indicates that the total interaction energy at a particular location depends on the relative proportions of cells

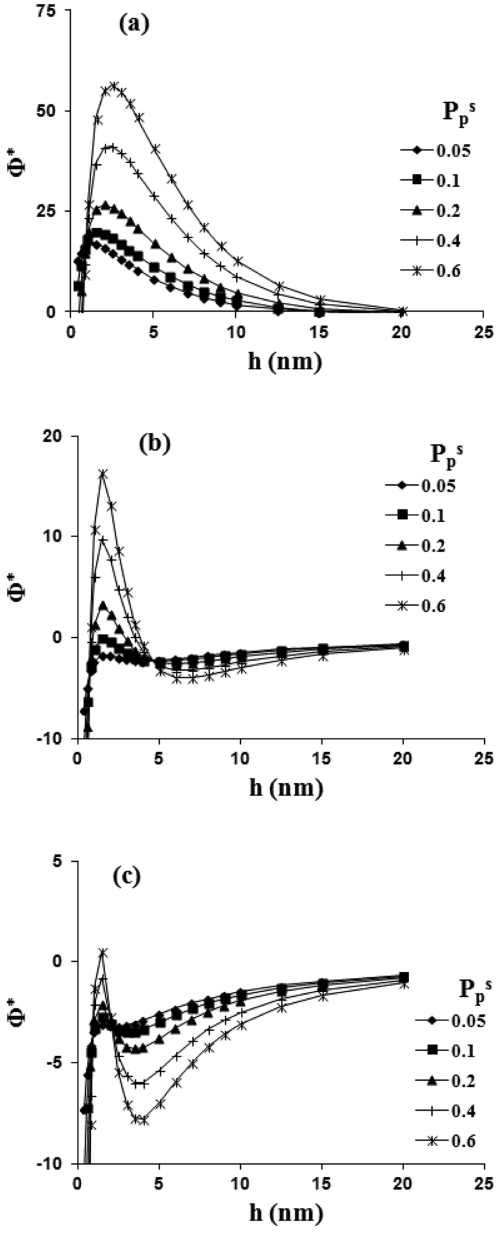

Figure 3. Simulated values of Φ* as a function of h for various P_p^s (0.05, 0.1, 0.2, 0.4, and 0.6). The IS was 5.8 mM in (a), 50 mM in (b), and 100 mM in (c). Parameter values used in these simulations included ζ^s = −11.1 mV, r_c = 500 nm, A_h = 78.5 nm^2, and h_r^s = 10 nm.

dx.doi.org/10.1021/la400229f | Langmuir 2013, 29, 3668−3676

with and without pillars. Pillar tops provide a greater contribution to the total interaction energy as P_p^s increases because of the associated greater frequency of higher values of N_p^s. The value of $\Phi_s(h)$ on pillar tops is also higher than $\Phi_s(h + h_r^s)$ on cells without pillars. Consequently, increases in P_p^s produced an increase in the magnitude of Φ_{max}* and Φ_{2min}* in Figure 3. Primary minimum interactions tended to occur for higher h_r^s and lower P_p^s values, e.g., for isolated pillars. Note that Φ_{max}* and Φ_{2min}* were highest on completely smooth surfaces that occurred when $P_p^s = 1$. Consequently, the magnitude of Φ_{max}* and Φ_{2min}* increased as P_p^s increased and approached a smooth surface (i.e., pillars cover almost all the surface). Similar to homogeneous surfaces, this increase in the depth of Φ_{2min}* with P_p^s was enhanced at higher IS. These trends are consistent with previous findings,[7,19,23] although these studies have not systematically investigated the effects of P_p^s or determined upscaled values of Φ*.

The values of h_r^s and P_p^s also had a strong influence on the depth of the Φ_{1min}*. This effect was not very apparent in Figures 2 and 3 because Φ_{1min}* occurred when h was around 0.4 nm. Figure 4 shows plots of Φ_{1min}* as a function of h_r^s using

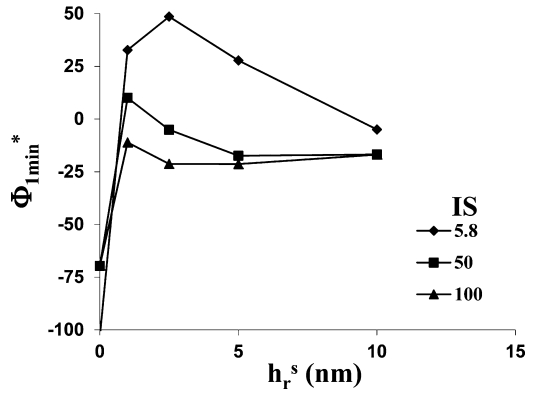

Figure 4. Simulated values of Φ_{1min}* as a function of h_r^s for various IS (5.8, 50, and 100 mM) conditions. Parameter values used in these simulations included r_c = 500 nm, ζ^s = −11.1 mV, A_h = 78.5 nm^2, and P_p^s = 0.196.

the same model parameters as in Figure 2. The depth of Φ_{1min}* varies in a nonlinear fashion with h_r^s. The maximum depth of Φ_{1min}* occurred in the absence of roughness. Increasing h_r^s initially produced an increase in Φ_{1min}*, and sometimes positive values of Φ_{1min}* (repulsive interaction energy), as a result of the combined effect of Born repulsion and surface roughness. However, further increases in h_r^s produced a decrease in Φ_{1min}* due to the dominant effect of van der Waals attraction and the electric double layer. It should be emphasized that finite values of Φ_{1min}* > −21.4 occurred when h_r^s > 0, even in the absence of an energy barrier to attachment (e.g., when the IS = 100 mM). In addition, the depth of Φ_{1min}* increased with IS. Consequently, Φ_{1min}* behaves in many ways like a deep Φ_{2min}*. Similar to Φ_{2min}* (Figure 3), the depth of Φ_{1min}* increased (became more negative) with P_p^s (data not shown).

Figure 5 presents plots of Φ* and the standard deviation of Φ* (σ_Φ) as a function of h for various A_h (10, 100, 500, 1000, and 5000 nm^2) and IS (5.8 and 50 mM). Specific parameter values used in these simulations included ζ^s = −11.1 mV, r_c = 500 nm, P_p^s = 0.196, and h_r^s = 10 nm. The mean values of Φ* do not change with A_h (Figure 5a). In contrast, σ_Φ was strongly dependent on A_h, h, and IS. In particular, σ_Φ increased with

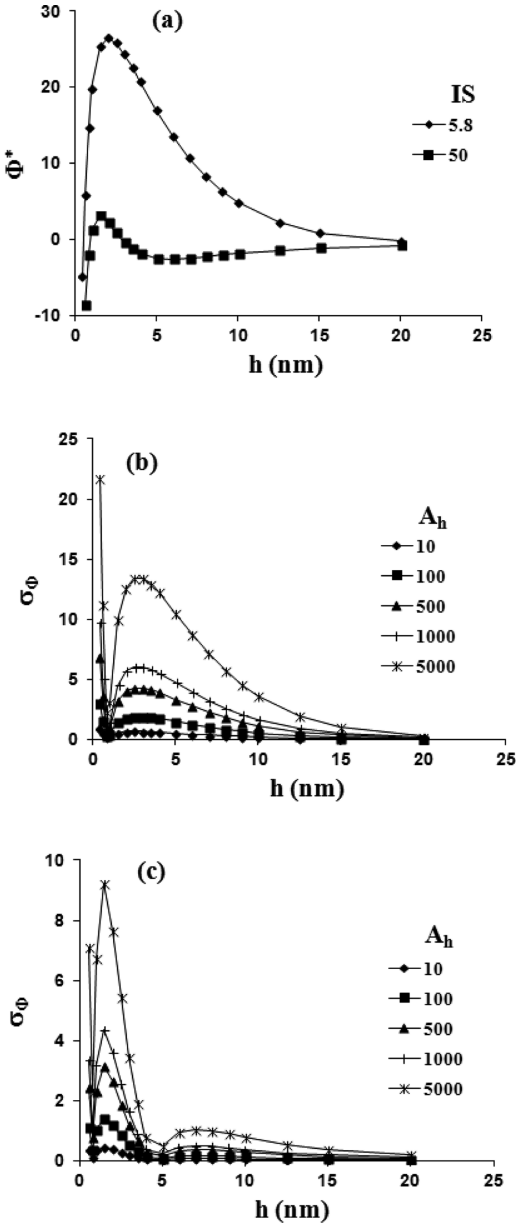

Figure 5. Simulated values of Φ* (a) and σ_Φ (b, c) as a function of h for various A_h (10, 100, 500, 1000, and 5000 nm^2). The IS equaled 5.8 mM in (b) and 50 mM in (c). Other parameter values were ζ^s = −11.1 mV, r_c = 500 nm, P_p^s = 0.196, and h_r^s = 10 nm.

larger A_h and $|\Phi^*(h)|$ and smaller IS. A value of $\sigma_\Phi > 0$ implies spatial variations in $\Phi(h)$, which produces a corresponding horizontal component of the adhesive force and a resisting torque which are essential for colloid immobilization in the presence of fluid flow.[48,49]

Colloid immobilization in Φ_{2min}* has recently been debated in the literature.[50,51] Note that $\sigma_\Phi > 0$ occurs for Φ_{2min}* in this example. Consequently, Figure 5 supports the potential for colloid immobilization in Φ_{2min}*. Collectively, Figures 2−5 demonstrate that microscopic variations in surface roughness that are present on all natural surfaces will produce a horizontal component of the adhesive force that will influence colloid immobilization and/or release with changes in IS. Values of A_h had a large influence on σ_Φ (Figure 5). However, values of h_r^s and P_p^s also influenced σ_Φ, but to a lesser extent. In general, σ_Φ

dx.doi.org/10.1021/la400229f | Langmuir 2013, 29, 3668−3676

increased with h_r^s but varied in a more complex manner with P_p^s (data not shown).

Figure 6 presents plots of Φ* and σ_Φ as a function of h for various r_c (250, 500, 1250, and 2500 nm) at IS = 50 mM.

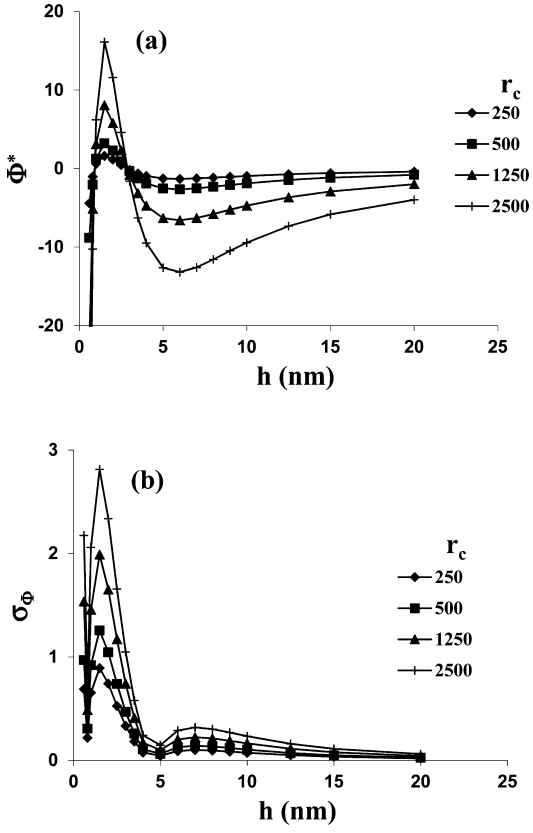

Figure 6. Simulated values of Φ* (a) and σ_Φ (b) as a function of h for various r_c (250, 500, 1250, and 2500 nm) at IS = 50 mM. Other parameter values included ζ^s = −11.1 mV, A_h = 78.5 nm^2, P_p^s = 0.196, and h_r^s = 10 nm.

Specific parameter values used in these simulations included ζ^s = −11.1 mV, A_h = 78.5 nm^2, P_p^s = 0.196, and h_r^s = 10 nm. As expected, the values of Φ_{max}* and Φ_{2min}* increased and decreased, respectively, with increasing r_c. More importantly, values of σ_Φ also increased with r_c. This implies greater values of the horizontal component of the adhesive force with r_c. However, colloid immobilization and release depends on the balance of applied hydrodynamic and resisting adhesive torques.[12,27,32,52−54] The fluid drag force and corresponding applied hydrodynamic torque increases with r_c,[12] so the influence of r_c on colloid immobilization cannot be ascertained without information about pore-scale variations in fluid velocity.

Physical Heterogeneity versus Chemical Heterogeneity. Figure 7 presents plots of Φ* and σ_Φ as a function of h when the SWI was homogeneous, physically heterogeneous, or chemically heterogeneous. The homogeneous simulation employed values of ζ^s = −11.1 mV, r_c = 500 nm, and IS = 50 mM. The physically heterogeneous simulation employed values of ζ^s = −11.1 mV, r_c = 500 nm, IS = 50 mM, A_h = 500 nm^2, P_p^s = 0.196, and h_r^s = 10 nm. The chemically heterogeneous model was a special case of the physically and chemically heterogeneous model described above when h_r^s = 0 nm. Other parameter values for the chemically heterogeneous simulation

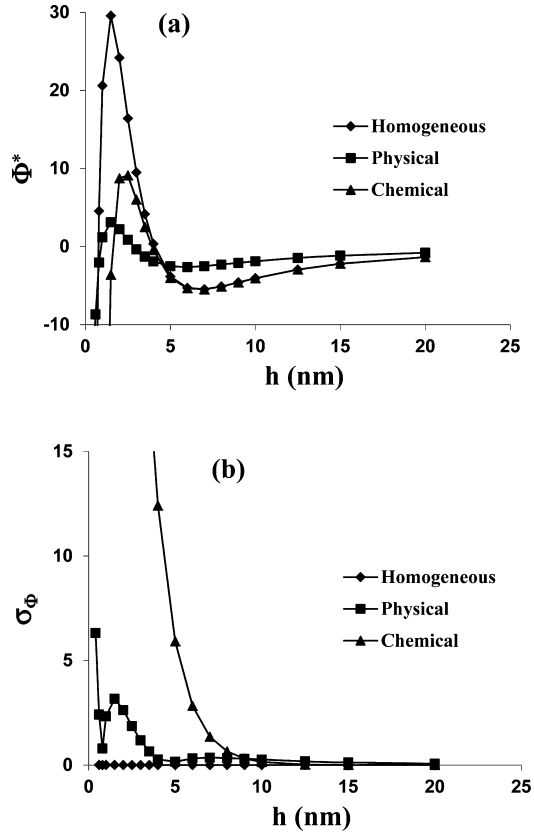

Figure 7. Simulated values of Φ* (a) and σ_Φ (b) as a function of h when the SWI was homogeneous, physically heterogeneous, or chemically heterogeneous and the IS = 50 mM. Parameter values were ζ^s = −11.1 mV for the homogeneous case; ζ^s = −11.1 mV, A_h = 500 nm^2, P_p^s = 0.196, and h_r^s = 10 nm for the physical heterogeneity case; and ζ_+^s = 54 mV, ζ_-^s = −27 mV, A_h = 500 nm^2, and P_+^s = 0.196 for the chemical heterogeneity case.

were ζ_+^s = 54 mV, ζ_-^s = −27 mV, IS = 50, A_h = 500 nm^2, and P_+^s = 0.196. Note that the mean value of ζ^s was the same for all the models, and values of P_p^s and P_+^s both equaled 0.196. Consequently, differences in the simulation results reflect the relative importance of physical (microscopic roughness) and chemical heterogeneities. As expected, both physical and chemical heterogeneity reduced values of Φ*(h) in comparison to the homogeneous case. Physical heterogeneity reduced Φ*(h) to a greater extent than a similar amount of chemical heterogeneity. Conversely, chemical heterogeneity had a much greater influence on σ_Φ than physical heterogeneity. This observation implies that chemical heterogeneity will have a greater effect on the horizontal component of the adhesive force that is involved in colloid immobilization and release. However, when the difference in ζ_+^s and ζ_-^s was decreased the values of σ_Φ were also decreased.

Physical and Chemical Heterogeneity on the SWI. Figure 8 presents plots of Φ* and σ_Φ as a function of h when the SWI was homogeneous or when the SWI had both physical and chemical heterogeneity. The homogeneous simulation employed values of ζ^s = −11.1 mV, r_c = 500 nm, and IS = 50 mM. The physically and chemically heterogeneous simulations both employed values of r_c = 500 nm, IS = 50 mM, A_h = 500 nm^2, P_+^s = 0.196, P_p^s = 0.196, and h_r^s = 10 nm. However, in one case random chemical heterogeneity was assumed with ζ_+^s = 54 mV and ζ_-^s = −27 mV. In the second case, the zeta potential of

dx.doi.org/10.1021/la400229f | Langmuir 2013, 29, 3668−3676

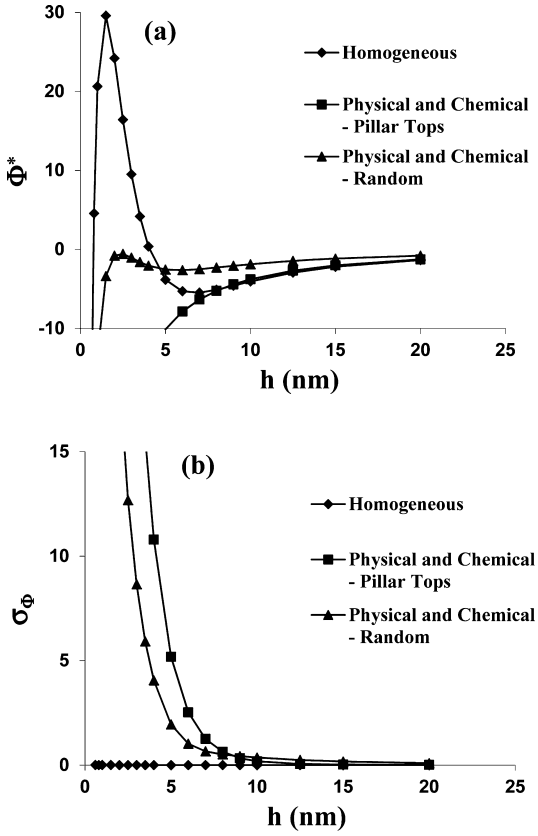

Figure 8. Simulated values of Φ* (a) and σ_Φ (b) as a function of h when the SWI was homogeneous or when the SWI had both physical and chemical heterogeneity and the IS = 50 mM. Parameter values were ζ^s = −11.1 mV for the homogeneous case. The two physically and chemically heterogeneous simulations employed values of A_h = 500 nm^2, P^s_+ = 0.196, P^s_p = 0.196, and h^s_r = 10 nm. In one case random chemical heterogeneity was assumed with ζ^s_+ = 54 mV and ζ^s_- = −27 mV, and in the second case the zeta potentials of the pillar tops (ζ^s_T = 54 mV) and bottoms (ζ^s_B = −27 mV) were different.

the pillar tops (ζ^s_T = 54 mV) and bottoms (ζ^s_B= −27 mV) was different. The mean value of ζ^s was the same again for the models. Note that combined physical and chemical heterogeneity produced a greater reduction in Φ*(h) than when only physical or chemical heterogeneity was considered (comparison of Figures 7 and 8). There was not a large difference in Φ*(h) values for the two cases of physical and chemical heterogeneity (pillar tops or random). However, values of Φ*(h) were more negative (favorable) and σ_Φ was somewhat larger when the positive zeta potentials were distributed on the pillar tops in comparison to randomly on the SWI.

CONCLUSIONS

Nanoscale surface roughness and charge heterogeneity has been widely recognized to influence colloid retention and release.[4−8,10,14,16,23] However, previous publications have not yet reported the mean and variance of Φ* on physically and chemically heterogeneous solid surfaces at the REA scale. The approach of Bradford and Torkzaban[37] was extended in this work to overcome these limitations. This information is needed to better understand and predict colloid interactions and retention in natural environments. Simulation results were validated by comparison with published Monte Carlo simulations using the grid surface integration technique.[16]

The mean and variance of Φ* were strong functions of the roughness parameters. Increasing the fraction of the roughness on the solid increased the magnitude of Φ_{max}* and Φ_{2min}*, whereas increasing the roughness height reduced the magnitude of Φ_{max}* and Φ_{2min}*. Primary minimum interactions tended to occur on isolated roughness pillars, but their depths were shallow as a result of Born repulsion. Conversely, the secondary minimum was strongest on smooth surfaces. The variance in Φ* increased with the colloid size, the magnitude of Φ*, height of the roughness, and especially and size (cross-sectional area) of the heterogeneity. The variance of Φ_{2min}* was greater than zero on heterogeneous surfaces, especially at higher IS and for larger colloids. This implies the presence of a tangential component of the adhesive force and a resisting torque that controls immobilization and release for colloids interacting in a secondary minimum.

Physical and/or chemical heterogeneity reduced the magnitude of Φ* in comparison with the corresponding homogeneous situation. In general, physical heterogeneity had a greater influence on mean properties of Φ* than similar amounts of chemical heterogeneity. However, the largest reduction in the mean value of Φ* occurred on surfaces with both physical and chemical heterogeneity. The variance in Φ* tended to be greatest on surfaces with chemical heterogeneity.

AUTHOR INFORMATION

Corresponding Author

*Phone 951-369-4857; e-mail Scott.Bradford@ars.usda.gov.

Notes

The authors declare no competing financial interest.

ACKNOWLEDGMENTS

This research was supported by the USDA, ARS, NP 214.

REFERENCES

(1) Derjaguin, B. V.; Landau, L. D. Theory of the stability of strongly charged lyophobic sols and of the adhesion of strongly charged particles in solutions of electrolytes. *Acta Physicochim. URSS* **1941**, *14*, 733−762.

(2) Verwey, E. J. W.; Overbeek, J. Th. G. *Theory of the Stability of Lyophobic Colloids*; Elsevier: Amsterdam, 1948.

(3) Suresh, L.; Walz, J. Y. Effect of surface roughness on the interaction energy between a colloidal sphere and a flat plate. *J. Colloid Interface Sci.* **1996**, *183*, 199−213.

(4) Bhattacharjee, S.; Elimelech, M. Surface element integration: A novel technique for evaluation of DLVO interaction between a particle and a flat plate. *J. Colloid Interface Sci.* **1997**, *193*, 273−285.

(5) Bhattacharjee, S.; Ko, C.-H.; Elimelech, M. DLVO interaction between rough surfaces. *Langmuir* **1998**, *14*, 3365−3375.

(6) Hoek, E. M. V; Bhattacharjee, S.; Elimelech, M. Effect of membrane surface roughness on colloid-membrane DLVO interactions. *Langmuir* **2003**, *19*, 4836−4847.

(7) Hoek, E. M. V.; Agarwal, G. K. Extended DLVO interactions between spherical particles and rough surfaces. *J. Colloid Interface Sci.* **2006**, *298*, 50−58.

(8) Huang, X.; Bhattacharjee, S.; Hoek, E. M. V. Is surface roughness a "scapegoat" or a primary factor when defining particle-substrate interactions? *Langmuir* **2010**, *26*, 2528−2537.

(9) Kozlova, N.; Santore, M. M. Manipulation of micrometer-scale adhesion by tuning nanometer-scale surface features. *Langmuir* **2006**, *22*, 1135−1142.

(10) Duffadar, R. D.; Davis, J. M. Interaction of micrometer-scale particles with nanotextured surfaces in shear flow. *J. Colloid Interface Sci.* **2007**, *308*, 20−29.

(11) Santore, M. M.; Kozlova, N. Micrometer scale adhesion on nanometer-scale patchy surfaces: Adhesion rates, adhesion thresholds, and curvature-based selectivity. *Langmuir* **2007**, *23*, 4782−4791.
(12) Duffadar, R. D.; Davis, J. M. Dynamic adhesion behavior of micrometer-scale particles flowing over patchy surfaces with nanoscale electrostatic heterogeneity. *J. Colloid Interface Sci.* **2008**, *326*, 18−27.
(13) Kalasin, S.; Santore, M. M. Hydrodynamic crossover in dynamic microparticle adhesion on surfaces of controlled nanoscale heterogeneity. *Langmuir* **2008**, *24*, 4435−4438.
(14) Martines, E.; Csaderova, L.; Morgan, H.; Curtis, A. S. G.; Riehle, M. O. DLVO interaction energy between a sphere and a nanopatterned plate. *Colloids Surf., A* **2008**, *318*, 45−52.
(15) Duffadar, R. D.; Kalasin, S.; Davis, J. M.; Santore, M. M. The impact of nanoscale chemical features on micron-scale adhesion: Crossover from heterogeneity-dominated to mean-field behavior. *J. Colloid Interface Sci.* **2009**, *337*, 396−407.
(16) Bendersky, M.; Davis, J. M. DLVO interaction of colloidal particles with topographically and chemically heterogeneous surfaces. *J. Colloid Interface Sci.* **2011**, *353*, 87−97.
(17) Ma, H. L.; Pazmino, E.; Johnson, W. P. Surface heterogeneity on hemispheres-in-cell model yields all experimentally-observed non-straining colloid retention mechanisms in porous media in the presence of energy barriers. *Langmuir* **2011**, *27*, 14982−14994.
(18) Henry, C.; Minier, J.-P.; Lefevre, G.; Hurisse, O. Numerical study on the deposition rate of hematite particle on polypropylene walls: Role of surface roughness. *Langmuir* **2011**, *27*, 4603−4612.
(19) Shen, C.; Li, B.; Wang, C.; Huang, Y.; Jin, Y. Surface roughness effect on deposition of nano- and micro-sized colloids in saturated columns at different solution ionic strengths. *Vadose Zone J.* **2011**, *10*, 1071−1081.
(20) Shen, C.; Wang, L.-P.; Li, B.; Huang, Y.; Jin, Y. Role of surface roughness in chemical detachment of colloids deposited at primary energy minima. *Vadose Zone J.* **2012**, DOI: 10.2136/vzj2011.0057.
(21) Shen, C.; Lazouskaya, V.; Zhang, H.; Wang, F.; Li, B.; Jin, Y.; Huang, Y. Theoretical and experimental investigation of detachment of colloids from rough collector surfaces. *Colloids Surf., A* **2012**, *410*, 98−110.
(22) Shen, C.; Lazouskaya, V.; Jin, Y.; Li, B.; Ma, Z.; Zheng, W.; Huang, Y. Coupled factors influencing detachment of nano- and micro-sized particles from primary minima. *J. Contam. Hydrol.* **2012**, *134*−*135*, 1−11.
(23) Shen, C.; Wang, F.; Li, B.; Jin, Y.; Wang, L.-P.; Huang, Y. Application of DLVO energy map to evaluate interactions between spherical colloids and rough surfaces. *Langmuir* **2012**, *28*, 14681−14692.
(24) Elimelech, M.; Gregory, J.; Jia, X.; Williams, R. A. *Particle Deposition and Aggregation: Measurement, Modeling, and Simulation*; Butterworth-Heinemann: Oxford, England, 1995.
(25) Bowen, W. R.; Doneva, T. A. Atomic force microscopy studies of membranes: Effect of surface roughness on double-layer interactions and particle adhesion. *J. Colloid Interface Sci.* **2000**, *229*, 544−549.
(26) Bowen, W. R.; Doneva, T. A.; Stoton, A. G. The use of atomic force microscopy to quantify membrane surface electrical properties. *Colloids Surf., A* **2002**, *201*, 73−83.
(27) Das, S. K.; Schechter, R. S.; Sharma, M. M. The role of surface roughness and contact deformation on the hydrodynamic detachment of particles from surfaces. *J. Colloid Interface Sci.* **1994**, *164*, 63−77.
(28) Chen, G.; Bedi, R. S.; Yan, Y. S.; Walker, S. L. Initial colloid deposition on bare and zeolite-coated stainless steel and aluminum: Influence of surface roughness. *Langmuir* **2010**, *26*, 12605−12613.
(29) Shellenberger, K.; Logan, B. E. Effect of molecular scale roughness of glass beads on colloidal and bacterial deposition. *Environ. Sci. Technol.* **2002**, *36*, 184−189.
(30) Morales, V. L.; Gao, B.; Steenhuis, T. S. Grain surface-roughness effects on colloid retention in the vadose zone. *Vadose Zone J.* **2009**, *8* (1), 11−20.
(31) Bradford, S. A.; Kim, H. Causes and implications of colloid and microorganism retention hysteresis. *J. Contam. Hydrol.* **2012**, *138*−*139*, 83−92.
(32) Bradford, S. A.; Torkzaban, S.; Kim, H.; Simunek, J. Modeling colloid and microorganism transport and release with transients in solution ionic strength. *Water Resour. Res.* **2012**, *48*, 9.
(33) Harvey, R. W.; Garabedian, S. P. Use of colloid filtration theory in modeling movement of bacteria through a contaminated sandy aquifer. *Environ. Sci. Technol.* **1991**, *25*, 178−185.
(34) Sun, N.; Elimelech, M.; Sun, N.-Z.; Ryan, J. N. A novel two-dimensional model for colloid transport in physically and geochemically heterogeneous porous media. *J. Contam. Hydrol.* **2001**, *49*, 173−199.
(35) Schijven, J. F.; Simunek, J. Kinetic modeling of virus transport at the field scale. *J. Contam. Hydrol.* **2002**, *55*, 113−135.
(36) Grolimund, D.; Borkovec, M. Release of colloidal particles in natural porous media by monovalent and divalent cations. *J. Contam. Hydrol.* **2006**, *87*, 155−175.
(37) Bradford, S. A.; Torkzaban, S. Colloid adhesive parameters for chemically heterogeneous porous media. *Langmuir* **2012**, *28*, 13643−13651.
(38) Vaidyanathan, R.; Tien, C. Hydrosol deposition in granular media under unfavorable surface conditions. *Chem. Eng. Sci.* **1991**, *46*, 967−983.
(39) Song, L. F.; Johnson, P. R.; Elimelech, M. Kinetics of colloid deposition onto heterogeneously charged surfaces in porous media. *Environ. Sci. Technol.* **1994**, *28*, 1164−1171.
(40) Tufenkji, N.; Elimelech, M. Breakdown of colloid filtration theory: Role of the secondary energy minimum and surface charge heterogeneities. *Langmuir* **2005**, *21* (3), 841−852.
(41) Zhang, J.; Srvastava, S.; Duffadar, R.; Davis, J. M.; Rotello, V. M.; Santore, M. M. Manipulating microparticles with single surface-immobilized nanoparticles. *Langmuir* **2008**, *24*, 6404−6408.
(42) Hogg, R.; Healy, T. W.; Fuerstenau, D. W. Mutual coagulation of colloidal dispersions. *Trans. Faraday Soc.* **1966**, *62*, 1638−1651.
(43) Gregory, J. Approximate expression for retarded van der Waals interaction. *J. Colloid Interface Sci.* **1981**, *83*, 138−145.
(44) Ruckenstein, E.; Prieve, D. C. Adsorption and desorption of particles and their chromatographic separation. *AIChE J.* **1976**, *22*, 276−285.
(45) Jury, W. A.; Roth, K. *Transfer Functions and Solute Movement through Soils: Theory and Applications*; Birkhauser Verlag: Basel, Switzerland, 1990.
(46) Kuo, R. J.; Matijevic, E. Particle adhesion and removal in model systems. Part 2. Monodispersed chromium hydroxide on steel. *J. Chem. Soc., Faraday Trans.* **1979**, *75*, 2014.
(47) Grolimund, D.; Borkovec, M. Release of colloidal particles in natural porous media by monovalent and divalent cations. *J. Contam. Hydrol.* **2006**, *87*, 155−175.
(48) Czarnecki, J.; Warszynski, P. The evaluation of tangential forces due to surface inhomogeneities in the particle deposition process. *Colloids Surf.* **1987**, *22*, 207−214.
(49) Busscher, H. J.; Poortinga, A. T.; Bos, R. Lateral and perpendicular interaction forces involved in mobile and immobile adhesion of microorganisms on model solid surfaces. *Curr. Microbiol.* **1998**, *37*, 319−323.
(50) Johnson, W. P.; Li, X.; Tong, M.; Ma, H. Comment on "Transport and fate of bacteria in porous media: Coupled effects of chemical conditions and pore space geometry". *Water Resour. Res.* **2009**, *45*, W09603.
(51) Torkzaban, S.; Walker, S. L.; Bradford, S. A. Reply to Comment on "Transport and fate of bacteria in porous media: Coupled effects of chemical conditions and pore space geometry". *Water Resour. Res.* **2009**, *45*, W09604.
(52) Bergendahl, J.; Grasso, D. Colloid generation during batch leaching tests: mechanics of disaggregation. *Colloids Surf., A* **1998**, *135*, 193−205.

(53) Bergendahl, J.; Grasso, D. Prediction of colloid detachment in a model porous media: hydrodynamics. *Chem. Eng. Sci.* **2000**, *55*, 1523−1532.
(54) Bradford, S. A.; Torkzaban, S.; Wiegmann, A. Pore-scale simulations to determine the applied hydrodynamic torque and colloid immobilization. *Vadose Zone J.* **2011**, *10*, 252−261.